ELSEVIER

Tectonophysics 333 (2001) 179–198

TECTONOPHYSICS

www.elsevier.com/locate/tecto

Seismogenic patterns in the Taiwan region: insights from source parameter inversion of BATS data

Honn Kao*, Pei-Ru Jian

Institute of Earth Sciences, Academia Sinica, Taipei, Taiwan, ROC

Received 1 October 1999; revised 18 January 2000

Abstract

We systematically invert source parameters of 96 earthquakes that occurred in the Taiwan region between July 1995 and June 1998, using waveforms recorded by the newly established Broadband Array in Taiwan for Seismology (BATS). The results are utilized to delineate the seismogenic patterns associated with the regional tectonic processes between the Eurasia and Philippine Sea plates. In general, high seismicity is observed at five locations, including the Nan-ao basin (~24°N, ~122.4°E), near the Hualien area (~24.2°N, ~121.7°E), east of the Longitudinal Valley and within the Philippine Sea plate, the forearc region to the west of Lanshu, and the Okinawa trough. Events with focal depths less than 25 km scatter across a wide region from the Taiwan Strait to the Ryukyu and Luzon arcs, whereas events between 25 and 50 km concentrate offshore east of Taiwan. Most earthquakes that occurred beneath the Nan-ao basin are consistent with the northward subduction of the Philippine Sea plate along the plate interface. Events offshore east of the Longitudinal Valley and within the Philippine Sea plate are dominated by a compressional regime along the NW/NWW directions, whereas the Lanshu–Lutao forearc is characterized by E–W compression. Normal faults showing N–S extension are observed in the Okinawa trough where we observed a successive rotation of *T*-axes from N–S to NW–SE as the epicenters approach Taiwan, indicating a possible interaction between the extensional and compressional strain regimes there. Most events between 50 and 65 km depth within the subducted Philippine Sea plate beneath Ryukyu are in downdip extension with lateral compression approximately parallel to the strike of the slab. The depth where the state of strain switches from downdip extension to downdip compression is constrained at 110–125 km for the southernmost Ryukyu slab. Based on our results, we propose that the subducted Philippine Sea plate beneath NE Taiwan plays a significant role in the overall orogenic process of Taiwan. The lithospheric collision in Taiwan should consist of two major components: one is the well-recognized "arc–continent collision" that dominates the central and southern Taiwan and another the "slab–continent collision" that reigns in northern Taiwan. A cluster of earthquakes near Hualien suggests that an incipient west- or northwestward subduction of the Philippine Sea plate is currently taking place there. Alternatively, they can be interpreted to suggest that the steeply east-dipping Longitudinal Valley fault may have transformed, near Hualien, into a diffuse thrust zone, which eventually connects itself to the plate interplate beneath the southernmost Ryukyu arc. Earthquakes beneath Taiwan and the Taiwan Strait are compatible with the overall collision convergence and lateral extrusion. Nonetheless, the lateral extrusion is probably only a secondary feature in the tectonic processes of Taiwan.

Keywords: seismogenic patterns; lithospheric collision; orogenic process

* Corresponding author.

PII: S0040-1951(00)00274-2

1. Introduction

The occurrence of earthquakes and their source characteristics have been well recognized as the manifestation of the kinematics and dynamics of the lithosphere (Isacks et al., 1968; Dewey and Bird, 1970; Forsyth, 1983). In particular, different seismogenic structures usually represent responses of the plate to various tectonic settings. Consequently, delineation of the distribution and characteristics of seismogenic structures is one of the key observations to constrain a region's tectonic model.

Taiwan is located at the junction of two subduction systems, namely, the Ryukyu and Luzon arcs to the east and south, respectively (Fig. 1). The complex tectonic setting, along with the interaction between the Philippine Sea plate and Eurasia continent, makes Taiwan one of the regions on Earth with the highest seismic activity. Since the late 1960s when the theory of plate tectonics was first introduced, it has been widely accepted that the tectonic evolution of Taiwan results from the continuously northwestward movement of the Philippine Sea plate colliding with the margin of the Eurasia continent, i.e., the well-known arc–continent collision model (Angelier et al., 1986; Lu and Hsü, 1992; Suppe, 1980; Teng, 1990; Tsai, 1986; Tsai et al., 1977; Wu, 1978). However, details of the evolution are by no means resolved, as evident from the various models proposed in the literature and the heated debate over them (Chemenda et al., 1997; Ho, 1986; Hsu and Sibuet, 1995; Kao et al., 1998b; Lu and Hsü, 1992; Suppe, 1984; Teng, 1990; Tsai, 1986; Wu, 1978; Wu et al., 1997).

In 1992, the Institute of Earth Sciences, Academia Sinica, initiated a prospectus to establish the Broadband Array in Taiwan for Seismology (BATS). The network, joined by several domestic and foreign institutions, is designed to have 15 permanent stations covering an area of approximately 350 km × 400 km

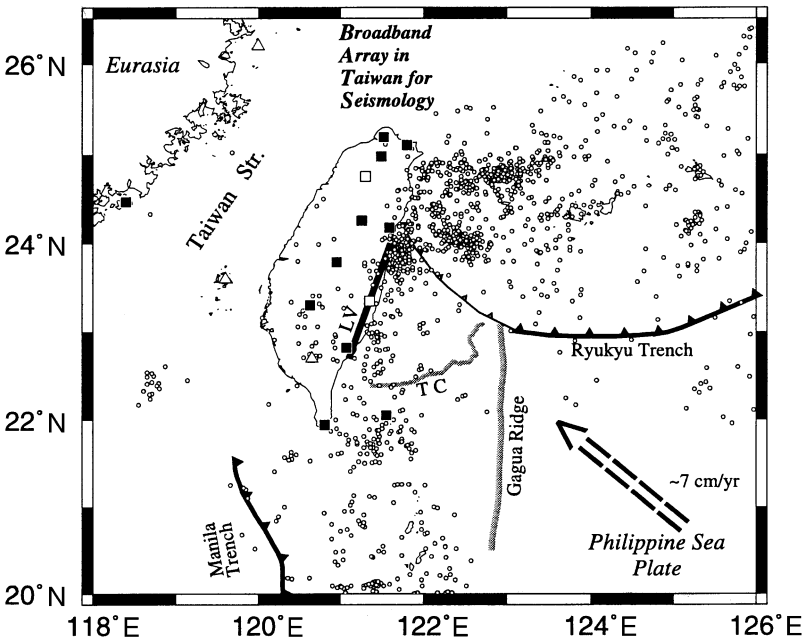

Fig. 1. Map showing the regional tectonic setting and station locations of the "Broadband Array in Taiwan for Seismology" (BATS). Solid and open squares represent stations currently in operation and in construction, respectively, while triangles are stations planned in the near future. Small open dots show earthquake epicenters that occurred in the region with $m_b \geq 4.5$ since 1980. Two subduction zones, the Ryukyu arc and Luzon arc, are located to the east and south, respectively. The bathymetric signature of the Ryukyu trench becomes less prominent to the west of ~123°E, as shown by a thinner line. The collision suture between the Philippine Sea and Eurasia plates is the Longitudinal Valley (LV) in east Taiwan, while the Taitung Canyon (TC) probably serves as a large-scale conjugate fault zone (Kao et al., 2000). The relative motion between the Philippine Sea and Eurasia plates (large arrow) is based on Seno et al. (1993).

(Fig. 1). There are an additional 15 portable units that can be deployed for intensive observations as needed. The network entered test operation in late 1994 and has produced high-quality data in sufficient quantity since early 1996 (Kao and Jian, 1999; Kao et al., 1998a).

One of the original goals of BATS is to systematically study source parameters of regional earthquakes in Taiwan. The conventional methods using P-wave polarities and/or amplitude ratios may result in large uncertainties in focal depths and ambiguous fault plane solutions, particularly for events that occur outside of the network. Unfortunately, the majority of earthquakes in Taiwan take place offshore east of the island (Fig. 1) where the station coverage is very poor. On the other hand, source parameters determined from inversion of teleseismic waveforms are only available for large and moderate-sized events, whose occurrence is much less frequent (e.g. Kao et al., 1998b, 2000). The advantage of using data from BATS lies in two aspects. First, the waveform inversion can be performed in a very low frequency band for events as small as $M_L \sim 4.5$, thus avoiding the effects of lateral heterogeneity, detailed velocity structures, and/or some hypocentral mislocations. More importantly, complete waveforms can provide much tighter constraints on not only earthquake fault plane solutions but also focal depths and seismic moments, even if the station coverage is not complete (e.g. Kao et al., 1998a). As a result, a large quantity of reliable source parameters can be systematically determined in order to obtain insights on the regional tectonics.

The purpose of this paper is three-fold. The first is to report earthquake source parameters inverted from BATS waveforms for the period between mid-1995 and mid-1998. Based on the results, we then delineate the regional seismogenic patterns, including the distribution of seismicity and the characteristics of focal mechanisms. Finally, we discuss the tectonic implications of our results. In particular, we address three issues: the significance of the subducted Philippine Sea plate in the regional orogeny, the subduction flip near the Hualien area, and the lateral extrusion of S. Taiwan in response to the collision.

2. Data and analysis

Continuous broadband waveforms are retrieved from BATS stations on a regular basis. The first step in data processing is to convert the format according to the Standard for Exchange of Earthquake Data (SEED) using software provided by IRIS. Event-oriented datasets are then extracted from the continuous SEED volumes based on the catalog reported by the Seismology Center of the Central Weather Bureau (CWB), Taiwan.

The description of the inversion algorithm is given in our previous studies and will not be repeated here (Kao and Jian, 1999; Kao et al., 1998a). Because the inversion relies primarily on long-period waveforms, which could not be efficiently generated by small events, we apply the algorithm to earthquakes with $M_L \geq 4.5$. The quality of inversion is evaluated by three parameters: the amount of isotropic component (ϕ), the misfit between the observed and synthetic waveforms (E), and the deviation from a pure double-couple source (i.e. the CLVD component, ε). For most events, the amount of isotropic component determined by inversion is quite insignificant. In the case of a larger ϕ, a priori constraint of $\phi \sim 0$ is imposed to stabilize the inversion process. A quality factor is assigned to each inversion result, ranging from A1 (the best) to F4 (the worst), according to the combination of E and ε. Detailed definition of the quality factor appears in Kao and Jian (1999).

3. Results

Because of various problems in the early stage of BATS, including insufficient number of stations, unexpected power and instrument failure, and high background noise level, etc., the inversion gives low-quality or even no solutions for many events before mid-1995. In this paper, we report results for earthquakes that occurred between July 1995 and June 1998 if they meet the following two criteria: (1) the inversion must utilize three-component waveforms from at least three stations, and (2) the quality of inversion must be at least higher than C4. In total, results for 96 earthquakes satisfy these conditions. The distribution of epicenters and inversion results are summarized in Fig. 2 and Table 1, respectively.

We summarize the inversion results in three figures according to the earthquakes' focal depths (Fig. 3a: 0–25 km, Fig. 3b: 25–50 km, and Fig. 3c: >50 km).

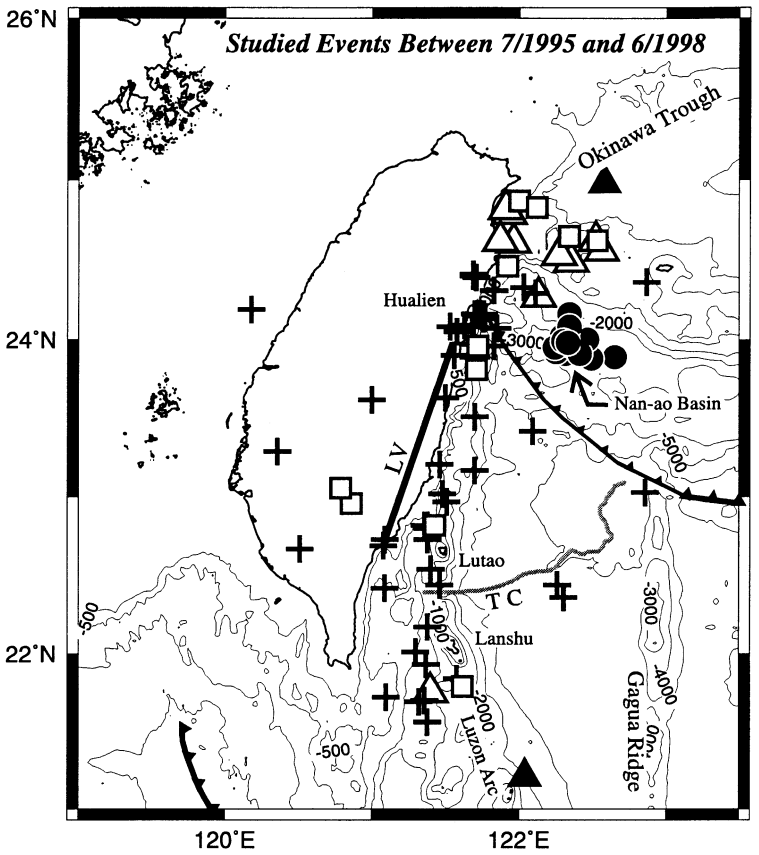

Fig. 2. Map showing the 96 earthquake epicenters included in this study. Different symbols represent events with distinct focal mechanism characteristics: solid circles, low-angle thrust; squares, normal; crosses, collisional thrust; open triangles, downdip extension; and solid triangles, downdip compression.

To make the text focused, here we try to outline the seismogenic characteristics and point out possible relationships among different structures. The complete set of our inversions is placed in Appendix A, which is available electronically from either the world-wide web or an anonymous ftp through Internet.

In general, the shallow seismicity (<25 km) scatters across a wide region from the Taiwan Strait to the Ryukyu and Luzon arc systems (Fig. 3a). For events deeper than 25 km, however, the vast majority takes place offshore east of Taiwan (Fig. 3b and c). Notice that the earthquake occurrence rate seems to be particularly high beneath the Nan-ao basin (~24°N, ~122.4°E), near the Hualien area (~24.2°N, ~121.7°E), east of the Longitudinal Valley and within the Philippine Sea plate, and in the forearc region to the west of Lanshu. The Okinawa trough also shows significant seismogenic activity.

3.1. Beneath the Nan-ao basin

All events beneath the Nan-ao basin show a consistent pattern of low-angle thrust focal mechanisms, except for event No. 2 (Fig. 3a) which is a high-angle thrust with *P*-axis oriented approximately parallel to the trench, i.e. lateral compression (Kao and Chen, 1991; Kao et al., 1998b). The distribution of hypocenters seems to show a trend of increasing depth northward (epicenters of events with depths between 25 and 50 km are located mostly to the north of those

Table 1
Source parameters of studied earthquakes

No.	O.T.[a]	Lat.[a]	Long.[a]	Depth	M_{xx}[b]	M_{yy}[b]	M_{zz}[b]	M_{xy}[b]	M_{yz}[b]	M_{xz}[b]	M_w[c]	Str.[d]	Dip[d]	Rake[d]	E[e]	ε[e]	ϕ[e]	QF[e]
1	95/07/05/17:33:48.6	24.83	122.12	27	−2.37	14.02	−9.54	−16.84	13.58	−1.93	4.87	354	49	−157	0.541	22.1	2.6	C2
2	95/08/15/14:53:56.7	23.98	122.43	18	−1.79	−4.87	8.62	2.87	0.80	3.47	4.55	43	37	112	0.540	29.1	6.8	C3
3	95/08/23/20:36:25.1	24.36	122.87	24	−1.64	0.11	1.16	0.65	0.01	−0.68	4.09	277	47	130	0.672	12.7	−6.5	C2
4	95/09/04/20:27:28.0	24.15	121.74	24	−0.92	−0.77	2.12	0.95	−0.47	−0.12	4.14	36	42	74	0.628	10.9	6.5	C2
5	95/10/04/05:01:48.0	24.87	122.00	24	0.35	1.95	−3.13	−4.46	2.31	1.77	4.45	4	60	−147	0.648	2.4	−4.5	C1
6	95/10/31/22:27:06.9	23.29	120.36	15	−0.34	−6.00	5.16	2.17	3.43	−0.64	4.50	176	42	52	0.535	16.8	−5.6	C2
7	95/11/10/21:07:51.6	22.82	121.38	12	8.33	−9.84	0.82	5.53	−4.77	−0.65	4.65	333	71	15	0.649	15.8	−1.9	C2
8	96/03/19/07:25:02.7	23.91	122.31	24	−14.77	7.95	10.49	−8.37	20.44	−5.26	4.89	325	30	154	0.654	22.6	4.6	C2
9	96/03/19/07:33:26.6	23.92	122.25	33	−24.02	20.38	2.47	−14.59	22.28	−18.64	5.00	327	44	174	0.652	25.1	−0.9	C3
10	96/03/28/17:53:19.2	24.02	122.29	27	−19.33	10.20	11.11	−2.83	16.50	−7.82	4.87	312	33	151	0.594	32.1	2.5	C2
11	96/03/29/03:28:53.5	23.97	122.33	24	−305.90	103.30	233.65	2.53	127.00	−76.65	5.61	292	37	126	0.583	37.3	3.1	C3
12	96/04/10/14:14:49.6	22.97	121.51	24	0.14	−1.67	1.26	0.73	−0.96	0.96	4.16	356	30	52	0.344	25.9	−3.7	B3
13	96/05/05/16:21:27.4	23.96	122.36	27	−4.52	2.06	2.91	−1.73	2.47	−1.82	4.38	319	48	153	0.544	29.5	3.5	C3
14	96/05/28/21:53:22.4	24.05	121.58	24	−4.90	−0.50	6.81	12.27	0.04	7.42	4.73	90	53	158	0.544	31.8	2.9	C3
15	96/07/06/01:27:05.5	22.67	120.51	24	−0.71	0.83	−0.65	−1.73	0.17	1.32	4.19	257	53	−8	0.520	26.5	−7.6	C3
16	96/07/17/09:26:56.6	23.90	122.48	24	−2.96	0.52	3.11	1.23	3.61	−1.73	4.41	262	20	106	0.535	23.2	4.3	C2
17	96/07/27/00:26:39.5	24.33	122.03	21	2.46	−4.33	2.71	−2.93	10.76	−13.81	4.78	132	14	8	0.397	30.0	1.4	B3
18	96/07/29/20:20:53.5	24.49	122.35	63	4.63	−72.97	62.35	76.99	49.39	57.29	5.34	66	51	148	0.352	16.4	−1.5	B2
19	96/08/05/18:41:13.5	23.17	121.70	45	0.46	−2.22	1.71	1.48	−1.48	−0.09	4.25	352	50	37	0.331	3.0	−0.6	B1
20	96/08/10/06:23:05.7	23.89	122.65	48	−241.58	72.30	195.17	41.06	299.59	−221.44	5.70	290	22	140	0.535	5.2	2.0	C1
21	96/09/01/15:55:41.8	24.46	121.92	27	0.36	−0.07	−0.03	−0.74	0.06	−0.47	3.91	97	58	−6	0.487	12.8	8.5	B2
22	96/09/05/18:12:47.2	24.53	122.27	57	−0.04	−0.62	0.46	0.02	0.23	0.47	3.86	19	27	122	0.282	9.2	−8.7	A1
23	96/09/06/02:04:56.4	21.93	121.37	24	21.92	−61.97	21.65	16.01	31.72	26.04	5.15	46	48	154	0.548	9.1	−8.8	C1
24	96/09/06/11:34:32.7	21.69	121.32	24	−8.14	−33.50	21.57	−16.08	22.98	−64.05	5.19	133	19	31	0.563	27.7	−8.8	C3
25	96/09/06/14:37:31.7	21.70	121.36	27	−0.77	0.39	0.09	−0.17	0.77	−0.60	3.98	318	32	170	0.587	5.3	−7.7	C1
26	96/09/09/01:52:38.6	24.31	121.83	15	−0.24	−1.29	1.06	−3.04	−1.64	1.58	4.34	282	63	27	0.408	24.1	−3.8	B2
27	96/10/01/07:54:24.9	22.96	120.86	18	1.5	3.81	−3.01	3.48	−1.73	−4.93	4.51	302	24	−125	0.450	36.2	9.0	B3
28	96/10/09/09:29:05.7	23.62	121.00	15	2.68	−1.76	−0.11	2.54	−1.30	−0.36	4.31	341	75	9	0.500	38.7	6.3	B3
29	96/11/01/09:08:03.8	23.21	121.46	18	−0.44	−1.57	1.74	0.84	−0.35	0.30	4.13	23	39	82	0.373	8.2	−4.4	B1
30	96/11/14/01:39:11.2	23.42	122.09	33	4.22	−9.01	4.49	1.62	−2.57	0.13	4.55	332	58	34	0.386	44.4	−1.1	B4
31	96/11/26/08:22:23.7	24.16	121.70	24	10.57	−8.18	5.20	−1.94	4.47	−30.67	4.95	131	11	31	0.547	39.5	7.7	C3
32	96/11/27/07:45:13.3	23.88	122.49	27	−3.22	1.10	2.26	−1.31	3.86	−0.77	4.41	317	27	143	0.618	25.9	0.9	C3
33	96/12/18/02:50:08.6	22.80	121.38	18	−0.09	−2.27	1.55	1.06	−1.52	0.88	4.24	356	34	45	0.424	9.8	−8.6	B1
34	96/12/18/11:20:23.2	22.82	121.36	18	−1.91	−2.49	5.17	2.48	−2.83	−1.62	4.45	19	46	53	0.472	46.3	3.8	B4
35	96/12/25/21:52:16.6	24.16	122.34	24	−8.51	2.10	8.30	0.41	4.93	−3.52	4.62	288	33	125	0.559	7.1	5.8	C1
36	96/12/28/21:08:06.5	24.00	122.46	42	−8.96	4.28	3.88	−3.85	15.20	−6.51	4.78	323	24	162	0.627	4.5	−1.4	C1
37	97/01/02/06:31:42.4	22.42	121.09	27	−0.03	−2.15	1.90	1.15	0.40	−2.66	4.30	221	22	118	0.543	23.6	−2.5	C2
38	97/01/05/10:34:16.9	24.62	122.53	27	55.50	−37.68	−14.57	38.03	30.55	−35.71	5.20	149	56	−17	0.535	25.0	1.3	C2
39	97/01/05/18:40:53.6	23.03	122.86	36	5.17	−6.56	0.75	4.48	−4.99	1.39	4.57	336	56	8	0.533	8.8	−2.4	C1
40	97/01/06/01:51:12.2	24.65	122.34	15	3.22	−1.04	−1.53	1.53	0.27	−1.52	4.29	252	58	−146	0.599	12.8	5.7	C2
41	97/01/16/01:07:20.4	22.01	121.30	27	−0.52	−7.70	5.07	27.05	−15.09	10.98	4.95	353	61	−4	0.433	65.5	−2.7	B4

Table 1 (*continued*)

No.	O.T.[a]	Lat.[a]	Long.[a]	Depth	M_{xx}[b]	M_{yy}[b]	M_{zz}[b]	M_{xy}[b]	M_{yz}[b]	M_{xz}[b]	M_w[c]	Str.[d]	Dip[d]	Rake[d]	E[e]	ε[e]	ϕ[e]	QF[e]
42	97/01/16/09:45:44.4	21.56	121.38	24	−0.78	−0.04	0.98	−0.73	0.21	1.78	4.15	276	27	29	0.353	33.2	2.3	B3
43	97/01/18/17:13:47.8	23.93	122.44	18	−8.93	3.37	12.66	−1.10	23.58	−9.23	4.90	295	15	133	0.613	7.1	7.8	C1
44	97/01/20/05:53:00.4	24.07	121.85	36	−0.37	−0.86	1.24	0.69	−0.24	0.76	4.06	46	31	108	0.287	9.8	0.3	A1
45	97/01/26/19:18:00.3	24.09	121.63	39	−0.40	0.70	0.09	1.31	0.39	−1.57	4.16	282	41	−179	0.418	6.2	5.8	B1
46	97/02/09/21:42:21.9	23.51	121.70	36	−0.05	−1.75	1.40	0.44	−0.33	−0.09	4.09	207	47	109	0.351	12.4	−7.2	B2
47	97/02/10/16:50:08.7	24.13	121.76	27	−0.55	0.39	0.23	1.32	0.64	−2.79	4.27	278	26	175	0.472	4.9	0.7	B1
48	97/02/13/08:29:54.2	23.21	121.46	18	0.10	−1.63	1.07	0.47	−0.75	−0.02	4.08	348	49	49	0.401	5.5	−8.6	B1
49	97/02/19/09:49:21.2	23.90	121.56	21	−1.35	−0.21	1.07	1.18	0.27	0.79	4.12	88	52	138	0.415	11.4	−7.7	B2
50	97/02/27/15:44:43.3	23.89	121.71	24	0.15	−1.40	1.98	0.88	−0.54	−2.04	4.24	227	29	136	0.371	14.3	7.6	B3
51	97/03/10/07:33:37.2	24.08	122.34	27	−11.88	6.16	7.29	−1.39	7.70	−5.81	4.71	309	39	151	0.441	17.5	3.6	B2
52	97/03/10/14:41:56.1	23.95	122.24	27	−5.10	2.24	5.35	−1.67	4.73	−2.41	4.53	310	33	140	0.516	4.2	9.8	C1
53	97/03/24/10:26:03.3	22.73	121.38	24	0.91	−1.31	0.18	0.50	−0.93	1.03	4.12	326	40	7	0.448	39.3	−3.5	B3
54	97/03/24/23:32:20.1	24.16	121.72	42	4.57	−3.85	0.62	−2.44	4.73	−5.46	4.56	124	34	1	0.419	27.7	4.6	B3
55	97/04/13/17:45:14.0	23.81	121.71	48	26.00	−9.71	−13.69	−0.46	14.85	−24.69	4.98	119	35	−25	0.578	35.6	2.3	C3
56	97/04/15/21:33:22.6	23.99	122.30	27	−6.39	3.44	2.64	−2.49	3.96	−3.58	4.54	321	46	160	0.565	6.7	−1.3	C1
57	97/04/27/23:59:32.6	24.61	121.96	60	−1.56	−0.32	1.83	4.15	0.90	3.09	4.43	87	54	159	0.541	8.2	−0.3	C1
58	97/05/02/21:30:23.6	24.19	120.18	27	1.30	−1.19	0.23	−0.51	−0.61	0.11	4.05	212	74	163	0.518	19.2	6.8	C2
59	97/05/03/02:46:13.7	22.54	121.40	27	18.60	−43.94	20.77	2.79	−19.45	4.82	5.02	328	54	33	0.423	11.0	−3.4	B2
60	97/05/15/10:43:47.7	24.79	121.93	108	−1.06	−0.03	0.31	−1.13	1.53	2.34	4.27	261	20	23	0.435	32.6	−7.3	B3
61	97/05/23/10:41:20.1	21.21	122.04	180	−1.62	5.73	−4.15	−2.99	3.46	4.11	4.54	231	43	−31	0.394	19.4	−0.1	B2
62	97/05/24/06:23:18.4	23.91	122.41	27	−0.77	0.50	0.12	−0.43	1.75	−0.92	4.15	328	21	174	0.610	4.2	−2.3	C1
63	97/05/31/23:21:37.4	24.62	121.87	60	−0.09	0.45	−0.01	0.20	1.82	0.76	4.14	197	10	−7	0.437	10.1	5.6	B2
64	97/06/14/19:25:20.2	23.89	121.70	21	0.22	−1.29	1.95	0.69	1.07	−1.78	4.23	192	21	74	0.507	11.3	9.9	C2
65	97/06/18/02:03:30.6	23.96	121.83	39	5.58	−14.99	6.98	5.70	3.66	8.74	4.75	51	43	152	0.379	37.9	−4.3	B3
66	97/06/22/09:36:04.1	22.17	121.38	21	8.38	−26.46	20.19	8.91	−8.23	−0.82	4.89	347	51	50	0.539	35.2	2.5	C3
67	97/06/27/15:53:27.5	21.84	121.58	36	−4.55	1.84	5.02	0.68	−4.36	5.13	4.55	109	27	144	0.551	20.9	8.1	C2
68	97/07/04/18:37:30.5	23.06	120.79	12	1.07	3.02	−9.56	10.00	−13.02	−12.76	4.83	327	16	−77	0.562	50.4	−8.1	C4
69	97/07/08/16:26:27.3	23.92	122.43	21	−8.65	4.48	0.91	−3.33	6.46	−3.14	4.62	327	44	170	0.633	21.9	−9.0	C2
70	97/07/10/08:19:53.6	21.79	121.62	15	3.77	5.42	−5.62	−0.17	−10.09	16.98	4.81	196	8	−103	0.526	26.1	5.7	C3
71	97/07/15/11:05:33.4	24.62	122.52	75	11.00	−21.97	9.19	15.14	3.43	161.80	5.41	63	6	155	0.426	12.9	−0.3	B2
72	97/08/05/08:41:13.5	23.02	121.48	21	0.10	−1.41	1.23	0.69	−1.06	0.66	4.13	356	33	46	0.476	8.3	−1.1	B1
73	97/09/08/16:17:07.5	24.08	121.69	27	−0.19	−0.32	0.91	1.00	0.08	−1.33	4.11	257	34	152	0.446	10.6	7.0	B2
74	97/10/11/18:24:25.7	24.98	122.58	129	−72.82	139.95	−66.20	41.04	−58.62	68.56	5.40	132	48	−156	0.427	16.5	0.2	B2
75	97/10/17/13:14:16.8	22.82	121.43	24	1.97	0.49	−1.80	1.98	−2.04	−0.32	4.29	332	33	−46	0.434	39.1	5.6	B3
76	97/10/22/11:16:26.6	22.44	121.46	33	4.93	−13.18	5.56	5.30	−6.73	0.63	4.69	339	55	29	0.376	10.2	−6.0	B2
77	97/10/25/02:40:15.9	24.29	122.11	36	−3.86	3.21	0.41	−0.55	0.83	−0.65	4.32	319	73	177	0.685	23.0	−1.9	C2
78	97/11/12/00:09:35.8	21.75	121.40	69	−6.17	−6.81	12.57	10.76	9.18	−15.80	4.86	242	22	119	0.408	28.3	−0.5	B3
79	97/11/12/22:36:45.2	24.14	121.77	30	−3.37	1.87	1.03	2.98	1.95	0.52	4.38	202	60	9	0.557	38.3	−3.0	C3
80	97/11/14/04:29:50.8	24.16	121.76	24	−5.29	−29.04	16.68	18.08	21.59	−40.78	5.10	209	16	91	0.499	35.1	−9.1	B3
81	97/12/23/02:35:45.7	23.98	122.33	30	−2.27	1.44	1.33	−1.55	3.28	−2.21	4.39	325	33	165	0.643	25.9	3.2	C3
82	98/01/18/19:56:51.7	22.73	121.09	15	−11.88	−17.73	45.08	26.36	28.87	−67.13	5.22	240	18	123	0.547	5.9	5.8	C1

Table 1 (*continued*)

No.	O.T.[a]	Lat.[a]	Long.[a]	Depth	M_{xx}[b]	M_{yy}[b]	M_{zz}[b]	M_{xy}[b]	M_{yz}[b]	M_{xz}[b]	M_w[c]	Str.[d]	Dip[d]	Rake[d]	E[e]	ε[e]	ϕ[e]	QF[e]
83	98/01/20/23:29:38.9	22.69	121.08	18	−0.44	−3.80	6.19	2.32	1.50	−7.59	4.59	219	19	113	0.552	3.8	6.3	C1
84	98/02/07/07:20:52.1	23.63	121.50	24	0.17	−0.95	0.59	0.49	−0.65	0.47	4.00	349	35	37	0.487	27.3	−4.4	B3
85	98/02/24/06:45:31.2	24.41	121.69	27	−0.29	−0.28	0.18	1.40	−0.02	−1.80	4.18	267	38	172	0.580	0.0	−5.4	C1
86	98/02/24/06:59:45.3	24.40	121.69	30	−0.30	0.38	−0.15	0.85	0.02	−0.52	3.95	281	60	−178	0.508	25.7	−2.4	C3
87	98/03/11/06:00:08.1	22.36	122.30	30	5.60	−4.15	−1.74	−0.47	2.39	−1.08	4.44	133	61	−5	0.551	61.1	−1.6	C4
88	98/03/11/17:21:54.9	22.44	122.26	30	33.38	−39.25	−1.34	2.99	1.86	6.36	4.98	48	81	−176	0.544	10.2	−6.0	C2
89	98/04/19/10:06:27.0	24.39	121.71	30	−0.20	0.20	−0.10	0.80	0.09	−1.36	4.07	277	31	−177	0.522	7.2	−2.0	C1
90	98/04/28/07:09:00.9	23.97	121.69	24	−0.10	0.11	0.07	0.07	0.44	−0.37	3.78	299	10	160	0.544	20.5	4.7	C2
91	98/05/02/00:05:53.0	21.72	121.10	24	2.07	−11.42	6.20	−0.42	3.49	0.30	4.60	25	51	130	0.629	22.2	−9.2	C2
92	98/05/02/05:37:42.4	24.56	122.56	84	−7.85	1.62	6.46	4.19	17.12	6.90	4.81	221	20	26	0.467	16.8	0.4	B2
93	98/05/09/20:53:39.0	24.82	121.91	72	0.63	−6.18	5.01	−3.09	11.05	6.02	4.70	6	21	150	0.434	14.9	−1.2	B2
94	98/05/15/08:50:28.5	23.96	121.72	39	1.60	−0.95	−0.74	−1.16	−0.87	1.34	4.19	291	43	−16	0.475	33.0	−1.3	B3
95	98/05/17/16:36:01.2	24.08	121.53	27	−0.59	−0.34	0.80	0.76	0.04	0.49	3.98	76	44	132	0.529	23.0	−3.3	C2
96	98/05/30/06:22:38.3	24.27	122.13	57	2.01	−8.81	6.33	3.00	3.99	4.75	4.62	44	42	141	0.429	4.0	−1.5	B1

[a] Origin time (O.T.: year/month/day/hour:minute:second) and epicentral locations (°N, °E) are reported by the Seismological Observation Center, Central Weather Bureau, Taiwan.

[b] x, y, and z point north, east, and vertically downward, respectively. All are in units of 1×10^{15} N m.

[c] Moment magnitude, defined as $M_w = (\log M_0/1.5) - 3.7$ where M_0 is the scalar seismic moment in N m.

[d] Estimated best double-couple solutions in degree.

[e] E, ε, ϕ, and QF are the average waveform misfit, the amount of CLVD component, the amount of isotropic component, and the overall quality factor, respectively, as defined in Kao and Jian (1999).

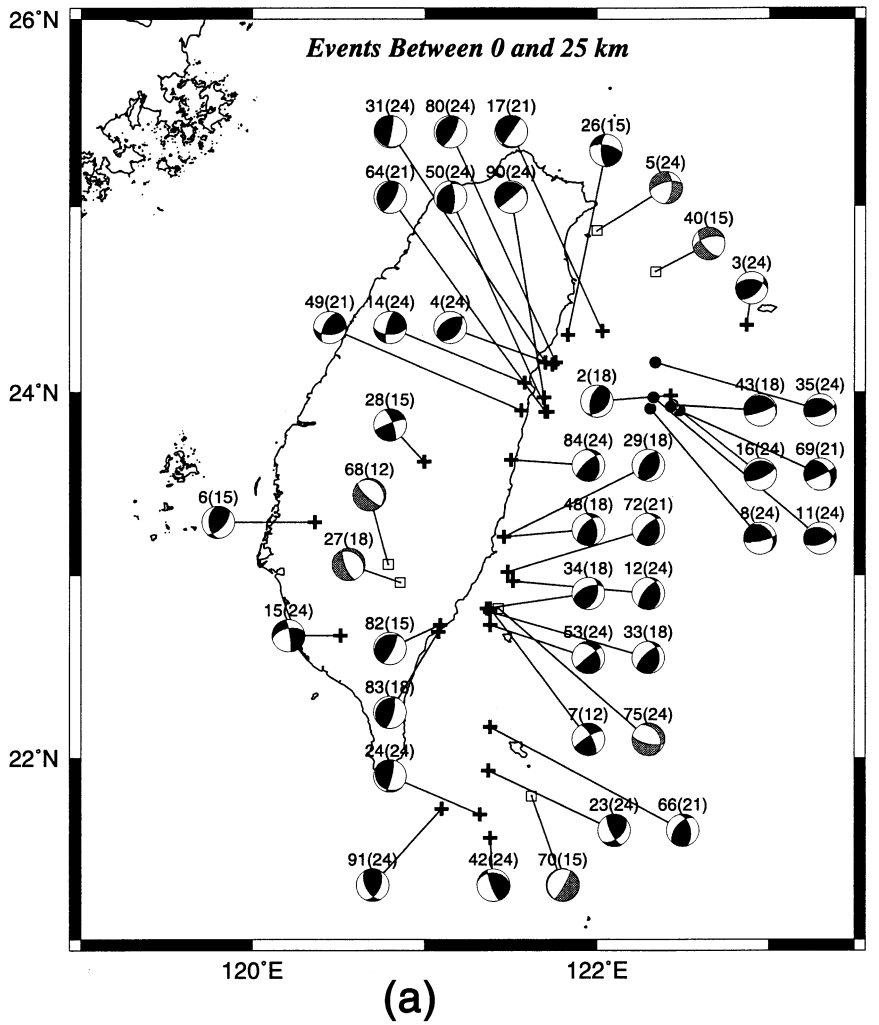

Fig. 3. (a) Epicenters and focal mechanisms of studied earthquakes with focal depths ≤25 km. Equal-area projections of the lower hemispheres of the focal spheres are plotted showing the orientation of nodal planes. Darkened areas show quadrants with compressional P-wave first motions. Distinct seismogenic patterns are indicated by different symbols and shadings for epicenters and inside the darkened quadrants, respectively, the same as those in Fig. 2. The two numbers above each fault plane solution show the event's number in Table 1 and its focal depth, respectively. Notice that the occurrence of shallow earthquakes is particularly frequent beneath the Nan-ao basin (~24°N, ~122.4°E) and near the Hualien area (~24.2°N, ~121.7°E). (b) Epicenters and focal mechanisms of studied earthquakes with focal depths between 25 and 50 km. Layout is the same as in Fig. 3a. Seismogenic patterns are similar to those shallower than 25 km, except that the intraplate interior of the Philippine Sea plate becomes seismically active while the corresponding region beneath Taiwan turns more aseismic. (c) Epicenters and focal mechanisms of studied earthquakes with focal depths >50 km. Layout is the same as in Fig. 3a. All events are associated with the two subducted slabs to the northeast and south, respectively. The deepest events (No. 74 in the Ryukyu slab and No. 61 in the Luzon slab) are in downdip compression, whereas all others are in downdip extension. Notice that events shallower than 65 km within the Ryukyu slab also show prominent compressional strain approximately parallel to the strike of the slab (i.e. lateral compression).

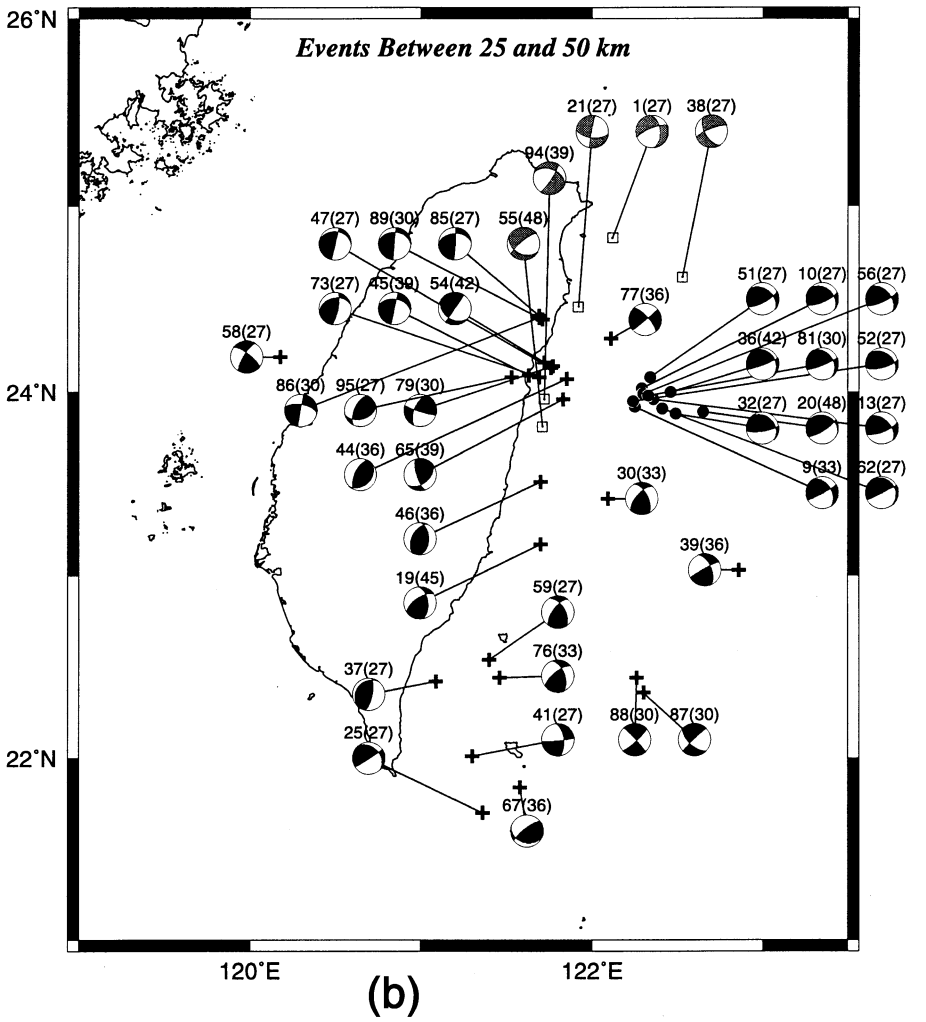

Fig. 3. (*continued*)

shallower than 25 km, Fig. 3a and b). This pattern seems to be more consistent with a seismogenic structure that is dipping gently toward the north or northeast, rather than a steeply dipping one toward the south. Consequently, given the patterns of focal mechanism and seismicity, the most straightforward interpretation would be that these events are the manifestation of relative slip along the interplate thrust zone.

The average azimuth of the slip vectors inferred from the low-angle thrust focal mechanisms is estimated to be 338 ± 12°. Such a value is significantly different from both the predicted relative plate motion, ~310° (Seno et al., 1993), and the trench normal, ~20° (Kao et al., 1998b), directions. Moreover, it confirms an earlier report of 345 ± 12° from events with $m_b \geq 5.5$ (Kao et al., 1998b). On the other hand, we found no significant difference (only ~2°) between the average slip vector directions for events shallower than 25 km and between 25 and 50 km.

3.2. Near the Hualien area

There are three distinct patterns of focal mechanisms

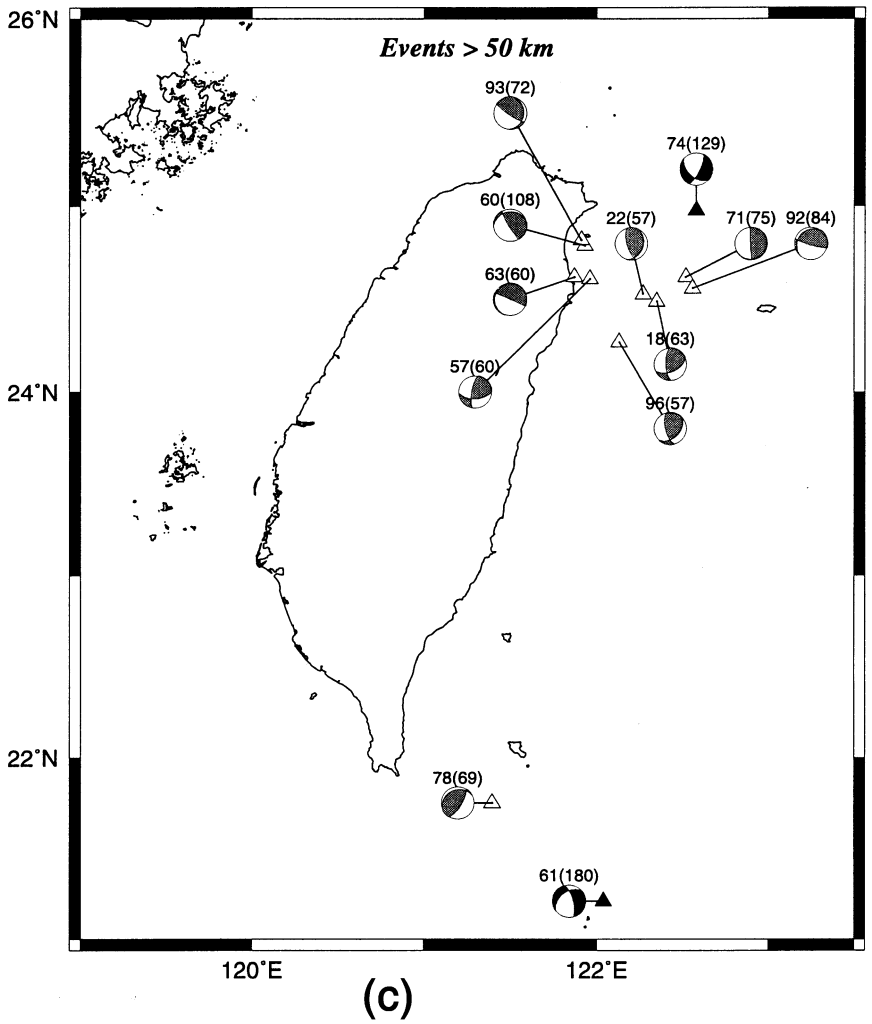

Fig. 3. (*continued*)

for the earthquake cluster near the Hualien area. The predominant one is characterized by thrust mechanisms with the eastern blocks overriding the west along nearly vertical nodal planes or the lower blocks moving westward relative to the upper, depending on the choice of fault planes (events No. 17, 31, 50, 64, 80, and 90 in Fig. 3a, and No. 45, 47, 54, 55, 73, 85, and 89 in Fig. 3b). These events are distributed between the depths of 21 (event No. 17) and 42 km (event No. 54).

Another interesting group shows consistent orientations of *P*-axes in the direction of relative plate motion (events No. 4, 14, and 49 in Fig. 3a, and No. 44, 65, 79, 86, and 95 in Fig. 3b). The *T*-axes, however, appear to have various orientations, ranging from nearly vertical (No. 4 and 44) to nearly horizontal (No. 14, 79, and 86). They can be adequately explained as the consequence of relative plate convergence in this region. Incidentally, the depth range of this earthquake group is about the same as that of the previous one (i.e. ~21–39 km).

One puzzling group, consisting of three events (No. 26 in Fig. 3a, and No. 21 and 94 in Fig. 3b), shows *T*-axes in the NW direction, a pattern that is the opposite of the known plate convergence. Because we found no

such pattern anywhere else in the studied region, it is suggested that their occurrence might be related to the complex interaction between the two plates (e.g. Kao et al., 1998b; Wu et al., 1997).

3.3. East of the longitudinal valley and within the Philippine Sea plate

The seismogenic pattern for this region is dominated by thrust events with the maximum compression in NW or NWW directions (events No. 7, 12, 29, 33, 34, 48, 53, 72, and 84 in Fig. 3a, and No. 19, 30, 39, and 46 in Fig. 3b). However, some of the mechanisms also have significant strike-slip components with *T*-axes roughly oriented N–S or NNE–SSW (No. 7, 30, and 39). Furthermore, we found one normal event (No. 75, Fig. 3a) showing NNE–SSW extension. The combination of these seems to suggest that the regional stress regime is dominated by the NWW–SEE convergence between the Philippine Sea plate and Eurasia and that there might be significant intraplate deformation within this portion of the Philippine Sea plate (Kao et al., 1998a).

In terms of the depth distribution, we found that the shallowest events (<25 km, Fig. 3a) all occurred close to the island's eastern coastline, whereas the deeper ones (25–50 km, Fig. 3b) are located away from the collision suture farther into the interior of the oceanic plate. Both the NW–SE compressional and NE–SW extensional regimes seem to exist at all depths, despite which the number of events showing extension is much less than that of those showing compression.

3.4. Lanshu–Lutao forearc and the Taitung Canyon

More than half of the sixteen events observed in this region show thrust or oblique-thrust mechanisms compatible with ~E–W compression (events No. 23, 24, 66, 82, 83, and 91 in Fig. 3a, and No. 37, 59, and 76 in Fig. 3b). Among them, four events (No. 24, 37, 82, and 83) have focal mechanisms similar to that observed in the earthquake cluster near Hualien. These seismogenic patterns are consistent with the inference from bathymetry and seismic profiling data that the northernmost Luzon forearc is closing due to the convergence between the Luzon arc and Taiwan (e.g. Fuh and Liu, 1998; Fuh et al., 1997; Lundberg et al., 1997).

Two strike-slip earthquakes are found beneath the Taitung Canyon between the Lanshu–Lutao volcanic arc and the Gagua Ridge (No. 87 and 88, Fig. 3b) and one to the west of Lanshu (No. 41, Fig. 3b). All three of them are compatible with the intraplate strain regime reported earlier (i.e. NW–SE compression and NE–SW extension) in the sense that the southern block is moving westward relative to the Taiwan collision zone (e.g. Kao et al., 2000; Yu et al., 1997).

Four events took place to the south of Lanshu with vertical dip-slip mechanisms (No. 42 and 70 in Fig. 3a, and No. 25 and 67 in Fig. 3b). This group is different from those mentioned earlier (No. 24, 37, 82, and 83) and in the Hualien area (No. 17, 31, 45, 47, 50, 54, 55, 64, 73, 80, 85, 89, and 90) by the distinct strikes of the vertical nodal planes. While most events with such mechanisms are striking N–S, these four events have nodal planes striking either NE–SW (No. 25, 67, and 70) or NW–SE (No. 42). They may be related to the local strain regime near the volcanic arc.

3.5. Beneath Taiwan and the Taiwan Strait

Events beneath the Central Range (events No. 27, 28, and 68 in Fig. 3a) all indicate N–S/NE–SW extension at shallow depth (<18 km). The strike-slip mechanism of event No. 28 is also compatible with the NWW–SEE compression that is found for the Coastal Plain in SW Taiwan (event No. 6, Fig. 3a). On the other hand, event No. 15 took place in the Pingtung Plain just west of the southern portion of the Central Range with the opposite orientation of *P*- and *T*-axes. If the N–S-striking nodal plane is taken as the actual fault plane, then the right-lateral strike-slip focal mechanism may imply that the southern portion of the Central Range and/or the Henchung Peninsula is currently extruding southward, probably in response to the intense collision to the north. In any case, the fact that events No. 28 and 15 exhibit opposite focal mechanism patterns clearly suggests a change in strain regime in between.

The only event that occurred in the Taiwan Strait (No. 58, Fig. 3b) shows *P*- and *T*-axes approximately in the E–W and N–S directions, respectively. The mechanism is compatible with the observed compression to the east on Taiwan and offshore and presumably indicates that the

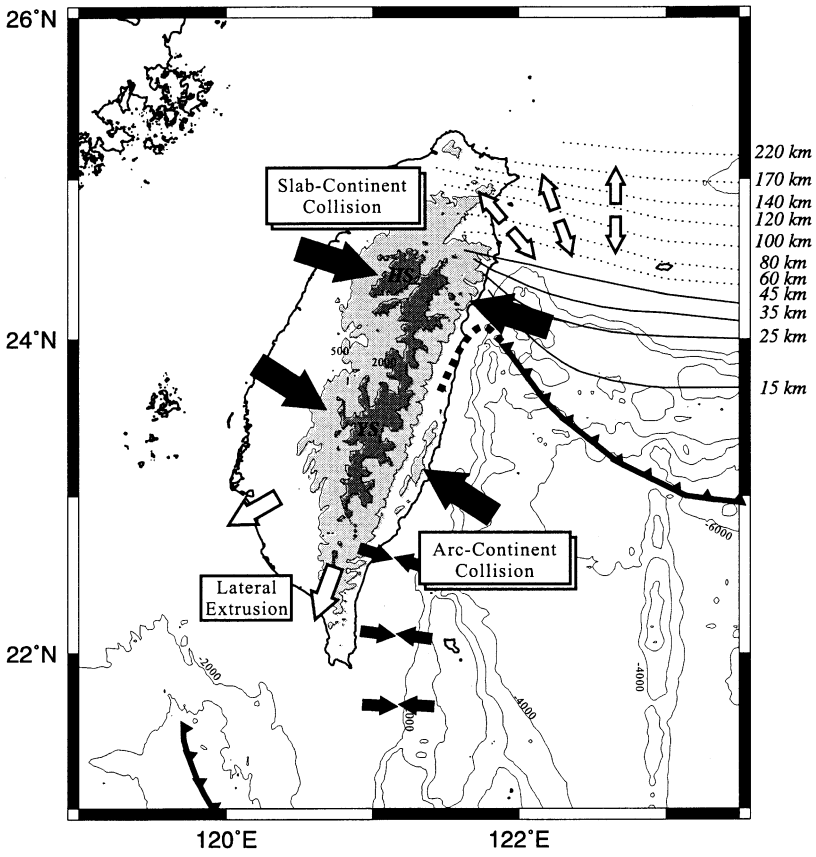

Fig. 4. Schematic diagram showing the tectonic implications of our results. Isodepths of the subducted slab and plate interface beneath the Ryukyu arc are adapted from Kao et al. (1998b) and shown by dotted and solid lines, respectively. Solid and open arrows represent the compressional and extensional strain regimes, respectively, inferred from our results. The lithospheric collision in Taiwan consists of at least two comparable components: one is the well-recognized "arc–continent collision" that dominates central and southern Taiwan and another the "slab–continent collision" that reigns in northern Taiwan (shown by the big solid arrows). Incidentally, the heights and sizes of the Hsuehshan (HS) and Yushan (YS) mountain systems in northern and central Taiwan are virtually equivalent and correspond to the western edge of the shallowest portion of the subducted Ryukyu slab and the northernmost end of the Luzon arc, respectively. Earthquakes near the Hualien area form a diffuse thrust zone that marks the transition from the Ryukyu trench to the collision suture along the Longitudinal Valley (thick dashed line). This diffuse zone may be interpreted as the formation of an incipient interface thrust zone in the Hualien area or, alternatively, the northward extension of the steeply east-dipping Longitudinal Valley fault. Prominent E–W compression is observed in the forearc region west of Lutao and Lanshu (pairs of small solid arrows). The direction of extension within the Okinawa trough shows a successive counterclockwise rotation as approaching Taiwan (pairs of open arrows). Lateral extrusion, probably in response to the collision between the two plates, is observed for south/southwest Taiwan (open arrows). However, it is probably a secondary feature in the overall tectonic processes of the region.

effect of lithospheric collision has reached far into the Taiwan strait (Wu et al., 1997). The direction of extension, on the other hand, is consistent with the large ($m_b = 6.5$) normal-faulting earthquake on September 16, 1994, near Penghu and probably represents the lateral extensional strain regime associated with a collision zone (e.g. Kao and Wu, 1996).

3.6. Earthquakes deeper than 50 km

A total of 12 events took place at depth greater than 50 km (Fig. 3c). Among them, only two are associated with the subducted slab beneath the Lutao–Lanshu arc (events No. 61 and 78), whereas the remaining 10 events belong to the Wadati-Benioff zone of the

subducted Philippine Sea plate beneath the Ryukyu arc. Although many previously proposed models discussing the regional tectonic evolution predict the possible existence of a remnant (or detached) slab beneath the Coastal Range and/or offshore east of Taiwan (e.g. Huang et al., 1997; Lu and Hsü, 1992; Teng, 1990), we observed no intermediate-depth earthquakes there.

All but two earthquakes that occurred in the Wadati-Benioff zone along the southernmost Ryukyu arc show focal mechanisms in downdip extension (events No. 18, 22, 57, 60, 63, 92, 93, and 96; Fig. 3c). Incidentally, most events with focal depths <65 km (No. 18, 22, 57, and 96) also have *P*-axes approximately parallel to the local strike of the trench, indicating that the shallowest portion of the subducted Philippine Sea slab is also under a lateral compressional strain regime (e.g. Kao and Chen, 1991; Kao et al., 1998b).

The deepest earthquakes in both subduction zones (No. 61 and 74, Fig. 3c) are in downdip compression, a pattern consistent with previous reports (e.g. Kao and Chen, 1991; Kao et al., 1998b, 2000). However, the exact depth where the state of strain within the subducted plate switches from extension to compression is loosely determined by previous studies to be somewhere between 110 and 260 km because of the large gap between the deepest downdip extensional and the shallowest downdip compressional events. With the new constraint from event No. 74, we are now able to redefine the strain-switching depth at 110–125 km for the southernmost Ryukyu slab.

3.7. Okinawa trough and the Ryukyu arc

We found four events in the Okinawa trough (No. 5 and 40 in Fig. 3a, and No. 1 and 38 in Fig. 3b). All of them show normal-faulting mechanisms with some oblique components. The *T*-axes of events No. 38 and 40 orient in ~N–S direction, consistent with the inferred opening direction of the trough (e.g. Miki et al., 1990; Sibuet et al., 1987, 1998). On the other hand, the maximum extension changes its direction to approximately NW–SE for events No. 1 and 5, which are located closer to Taiwan (Fig. 3a and b). This successive rotation of *T*-axes as approaching from the southern Okinawa trough to Taiwan confirms an earlier report based on large and moderate-sized events (Kao et al., 1998b).

Both events in the vicinity of Ryukyu arc (No. 3 in Fig. 3a, and No. 77 in Fig. 3b) indicate N–S compression. The one that is closer to Taiwan (No. 77) is compatible with an E–W direction of extension. This pattern is probably related to the complex interaction among various strain regimes between the southernmost Ryukyu arc and Taiwan, similar to the group of events No. 21, 26, and 94.

4. Tectonic implications and discussion

Although there are abundant reports in the literature that focused on the source parameters of earthquakes in the Taiwan region, it is not straightforward at all to extract internally consistent seismogenic patterns from the combined dataset owing to the various data types, methodology, and model assumptions. Inversion using waveforms recorded at teleseismic distances usually has good constraints on source parameters, but it also requires earthquakes of larger magnitude ($m_b > \sim 5.5$). Consequently, it takes several decades to accumulate a sufficient number of large and moderate-sized events to delineate the overall seismogenic patterns in the region (e.g. Kao et al., 1998b, 2000).

On the other hand, many studies indicate that the seismogenic patterns derived from earthquakes with smaller magnitudes seem to agree with those from bigger ones in general, although some effects from local heterogeneities are expected (e.g. Rau et al., 1996). Unfortunately, before the establishment of BATS, most focal mechanisms of smaller events in the Taiwan region are determined from the polarities of P-wave first motions and/or P/S amplitude ratios that depend critically on a well-distributed azimuthal coverage of seismic stations. Consequently, solutions for most offshore events may become ambiguous such that delineating detailed seismogenic patterns is difficult.

Taking advantage of the high-quality broadband waveforms of BATS, we extend the power of waveform inversion to the large number of smaller events in Taiwan and its vicinity. This study indicates that approximately the same amount of results can be obtained using just three years (7/1995–6/1998) of

BATS data as opposed to more than three decades of data from global networks. Of course, the short time window of BATS observation may not be sufficient to catch particularly large earthquakes, yet it seems justifiable to use our results to discuss general tectonic processes that persist in the region. In what follows, we try to point out some interesting tectonic insights from our results.

4.1. Slab–continent collision versus arc–continent collision

Since the late 1960s when the concept of plate tectonics became widely accepted, Taiwan's orogenic processes have been interpreted as the consequence of the collision between the northern Luzon arc of the Philippine Sea plate and the continental margin of the Eurasia plate (i.e. the so-called "arc–continent collision" model) (e.g. Angelier et al., 1986; Suppe, 1980; Teng, 1990; Tsai et al., 1977; Wu, 1978). Later in the 1980s, Suppe and co-workers in a series of studies proposed the "critical taper" model to explain the mechanics of the orogeny in Taiwan (Dahlen, 1988, 1990; Dahlen et al., 1984; Davis et al., 1983; Suppe, 1981). In this model, the tectonic deformation in Taiwan is confined above a basal decollement and is practically analogous to the wedge of soil that develops in front of a bulldozer. However, most recent geophysical evidences indicate that the orogeny probably has involved a significant portion of upper mantle and should be best regarded as the result of "lithospheric collision" between the two plates (e.g. Rau and Wu, 1995; Wu et al., 1997). Although this is a big step in redefining the overall tectonic framework in Taiwan, it does not specifically address the significance of the subducted slabs, in particular the subducted Philippine Sea plate beneath NE Taiwan where the strike of the slab is nearly perpendicular to the overall structural trend on the island. Whether and how the subducted Ryukyu slab affects the regional orogeny remains an untouched issue.

Our results clearly indicate that the Philippine Sea plate is dominated by strong E–W/NW–SE compression throughout its westernmost portion adjacent to Taiwan (Fig. 3). Before it enters the Ryukyu subduction zone, the compressional regime is revealed by a large number of thrust and oblique-thrust events (Fig. 3a and b). At greater depths, it is represented by the so-called "lateral compression seismic zone" revealed by a group of earthquakes with *P*-axes consistently parallel to the local strike of the slab (Fig. 3; Kao and Chen, 1991; Kao et al., 1998b). However, this group of events exists only at the shallowest portion ($\sim < 65$ km depth) of the subducted slab. Thus, from the collision's point of view, the effect on the Philippine Sea plate is not qualitatively different between the portion to the east of the Longitudinal Valley and the shallowest portion of the subducted slab. In other words, as long as the subducted slab is still in contact with the strongest portion of the Eurasia lithosphere, its involvement in the overall orogenic processes is probably similar to its counterpart before subduction.

We propose that the lithospheric collision in Taiwan consists of two major components: one is the well-recognized "arc–continent collision" that dominates central and southern Taiwan, and the other the "slab–continent collision" that reigns in northern Taiwan (Fig. 4). Indeed, this line of thinking may be incompatible with the inference that northern Taiwan is currently in the state of mountain collapsing (e.g. Teng, 1996). It is important to point out that such an inference is not based on precise geodetic or geophysical measurements on the rate of uplift and/or erosion over a period of time (unfortunately, even today such important information is still unavailable), but mainly on geological evidences that show extensional features (e.g. Crespi et al., 1996; Teng, 1996). We argue that the mountain-building here has probably reached a substantial scale such that these extension-related structures can be alternatively interpreted as the signs of gravitational sliding similar to those found in the central portion of the Central Range (e.g. Crespi et al., 1996; H.-T. Chu, personal communication, 1999) and high Tibet plateau (e.g. Armijo et al., 1986; Burchfiel and Royden, 1985; England and Houseman, 1989; Molnar and Tapponnier, 1978; Ratschbacher et al., 1994; Tapponnier et al., 1981). Moreover, recent seismic tomographic studies clearly show high-velocity

anomalies at the depth range of the upper crust beneath the eastern part of the Central Range, indicating a fast exhumation of deeper material throughout the Central Range (e.g. Lin et al., 1998; Ma et al., 1996; Rau, 1996). Combining the fact that the peak heights and sizes of the two major mountain systems in central and northern Taiwan (namely, the Yushan and Hsuehshan Ranges, respectively) are virtually equivalent (Fig. 4), it seems reasonable to infer that the slab–continent collision is at least as important as the arc–continent collision in Taiwan as far as the overall tectonic framework is concerned.

In addition to the slab–continent collision, the opening process of the Okinawa trough is another important factor in northern Taiwan. In fact, the extensional stress regime associated with the Okinawa trough, particular that in the I-lan plain, was cited by previous studies to argue for the collapse of mountain systems in northern Taiwan (e.g. Liu, 1995; Yeh et al., 1989). Such an inference, however, fails to acknowledge the fact that the effect of back-arc opening is, in fact, confined to regions above the subducted slab (Uyeda and Kanamori, 1979; Waschbusch and Beaumont, 1996). Since the intermediate-depth seismicity clearly indicates that the western edge of the subducted Philippine Sea plate coincides with the 121.5°E meridian (Kao et al., 1998b), it seems very unlikely that the entire mountain system in northern Taiwan (especially those to the west of 121.5°E such as the Hsuehshan Range) is currently collapsing due to the extensional process of the Okinawa trough.

4.2. The Hualien area: how does the polarity of subduction flip?

It has long been recognized that the two subduction systems near Taiwan have exactly opposite polarities: the Philippine Sea plate subducts beneath the Eurasia plate along the Ryukyu trench to the northeast, whereas the South China Sea block of the Eurasia plate goes beneath the Philippine Sea plate along the Manila trench to the south. Therefore, the flip of subduction polarity must somehow be accomplished in between. Seismic profiling data along the Longitudinal Valley indicate that the shallowest portion of the plate suture dips very steeply toward the east (Wang and Chen, 1997; Yu and Liu, 1989), making the Hualien area the most critical place to delineate exactly how the polarity flips. Unfortunately, observational constraints on this issue seem to be scarce in the literature.

Our results indicate that the seismogenic patterns near the Hualien area are very complex (Figs. 3 and 4). In addition to the thrust earthquakes with horizontal *P*-axes approximately in the collision direction, there are about an equal number of events showing mechanisms with one steeply and one shallowly dipping nodal plane. Such a mechanism pattern is very similar to that shown by the group of low-thrust events beneath the Hoping basin, except for a systematic counterclockwise rotation of ~45–90°. However, the hypocenters of these events do not seem to concentrate along any specific plane or surface, indicating that they may not be associated with a well-developed interface between the Philippine Sea and Eurasia plates.

One possible scenario is to interpret these events as a manifestation of forming a diffuse interface thrust zone in the Hualien area. In other words, an incipient west- or northwestward subduction of the Philippine Sea plate is currently taking place beneath the Hualien area such that the geometric relation between the two plates is reversed there with respect to the rest of the Longitudinal Valley. Although a similar inference has been suggested by previous studies based on results of physical modeling (e.g. Chemenda, 1995; Chemenda et al., 1997), further investigation is clearly required to prove the shallowly dipping nodal planes as the preferred fault planes.

An alternative is to take the steeply dipping nodal planes as the fault planes. In such a scenario, these earthquakes probably imply that the steeply east-dipping Longitudinal Valley fault may have transformed into a diffuse thrust zone near the Hualien area, as proposed by Angelier et al. (1995). This zone eventually connects itself to the plate interplate beneath the southernmost Ryukyu arc, which is represented by the low-angle thrust earthquake cluster beneath the Hoping basin. However, it is pointed out that occurrences of thrust events along near-vertical planes are mechanically difficult due to the large friction on the fault surface. Thus feasibility of such a configuration may be in question. As we pointed out

earlier, precise determination of the actual fault planes is probably the most critical test to distinguish between the proposed two scenarios.

4.3. Lateral extrusion of southern Taiwan

The existence of lateral extrusion behind a collision zone has been documented more than two decades ago (e.g. Molnar and Tapponnier, 1978; Ni and York, 1978; Tapponnier et al., 1981; Tapponnier and Molnar, 1977). Generally speaking, materials between a stable continental interior and the collision zone would respond to the convergence by moving along the direction of minimum stress, which is usually parallel to the major structural trend induced by the collision. In the case of Taiwan, the Longitudinal Valley is regarded as the present-day collision suture. Thus, the western Coastal Plain and the southern Hengchung peninsula are the likely regions where lateral extrusion is expected (Fig. 4).

Indeed, the most recent GPS surveys indicate that the velocity field of western Taiwan seems to have a systematic southwestward component increasing from north to south (e.g. Yu et al., 1997). This phenomenon of lateral extrusion is particularly prominent in SW Taiwan. However, geological surveys in SW Taiwan fail to find clear signs of lateral extrusion in the strata of Quaternary deformation (e.g. Lacombe et al., 1999). Marine morphology and seismic profiling surveys offshore SW Taiwan also provide no conclusive evidence (Liu et al., 1997). These two lines of contradictory observation seem to suggest that the lateral extrusion process, if any, must have developed only recently (e.g. Lacombe et al., 1999) — a conclusion compatible with the young history of collision in Taiwan.

In our results, there are only two shallow events occurring in SW Taiwan (events No. 6 and 15; Fig. 3a). The strike-slip mechanism of event No. 15 at a depth of 24 km is a clear indicator that significant shear motion of at least crustal scale exists. The *P*-axis is in the NE–SW direction, which is consistent with the fan-shaped distribution of principal compressive stress reported previously (e.g. Cheng, 1995; Hu et al., 1996; Yeh et al., 1991). The sense of motion suggests that either the Coastal Plain of SW Taiwan is currently moving westward or the southern Henchung Peninsula is moving southward with respect to the Central Range, depending on which nodal plane is the fault plane. Given the relatively less frequent occurrence of this particular kind of earthquake, we conclude that the lateral extrusion is probably only a secondary feature in the tectonic processes of Taiwan.

5. Conclusions

The complex tectonic framework in Taiwan consists of several major components: the southernmost Ryukyu subduction zone and Okinawa trough to the east, the northern Luzon arc–Manila trench system to the south, and the Taiwan collision zone in between. The frequent occurrence of earthquakes manifests the ongoing interaction between the Eurasia and Philippine Sea plates, yet delineation of the detailed distribution and characteristics of seismogenic structures in the region is difficult owing to the fact that the majority of seismic events took place outside of the regional network.

Taking advantage of the newly established Broadband Array in Taiwan for Seismology (BATS), we are able to extend the merit of waveform inversion to the large number of earthquakes with smaller magnitude. Three-component complete waveforms from at least three broadband stations are used in each inversion to ensure sufficient constraints on the results. In total, we systematically derive source parameters for 96 events that occurred in the region between July 1995 and June 1998.

Events with focal depths less than 25 km scatter across a wide region from the Taiwan Strait to the Ryukyu and Luzon arcs, whereas events between 25 and 50 km concentrate offshore east of Taiwan. In particular, high seismicity is observed at five locations, including the Nan-ao basin (~24°N, ~122.4°E), near the Hualien area (~24.2°N, ~127.7°E), east of the Longitudinal Valley and within the Philippine Sea plate, the forearc region to the west of Lanshu, and the Okinawa trough.

Most earthquakes that occurred beneath the Nan-ao basin show low-angle thrust focal mechanisms, consistent with the northward subduction of the Philippine Sea plate along the Ryukyu trench. Earthquakes near the Hualien area, on the other hand, show two seismogenic patterns. One is

characterized by thrust mechanisms with one nearly vertical and one horizontal nodal plane and another with consistent orientations of *P*-axes in the direction of relative plate motion. Events located to the east of the Longitudinal Valley and within the Philippine Sea plate are dominated by the maximum compression in NW or NWW directions with a few events also showing NNE extension. It is suggested that there might be significant intraplate deformation within this portion of the Philippine Sea plate.

In the Lanshu–Lutao forearc region, the seismogenic pattern is dominated by E–W compression with some vertical dip-slip events. Two strike-slip earthquakes are found beneath the Taitung Canyon between the Lanshu–Lutao volcanic arc and the Gagua Ridge. Another similar one is observed to the west of Lanshu. All three are compatible with the intraplate strain regimes reported earlier (i.e. NW–SE compression and NE–SW extension). Events beneath Taiwan and Taiwan Strait are compatible with the overall collision convergence. However, many events, particular those that occurred beneath the Central Range, also show prominent N–S extension. The opening of the Okinawa trough is evidenced by a group of normal events. Among them, we observed a successive rotation of *T*-axes from N–S to NW–SE as the epicenters approach Taiwan, indicating a possible interaction between the extensional and compressional strain regimes there. The Wadati-Benioff zone beneath the Ryukyu arc is much more active in terms of seismicity than that beneath the northern Luzon arc. Most events between 50 and 65 km depth within the subducted Philippine Sea plate beneath Ryukyu are in downdip extension with lateral compression approximately parallel to the strike of the slab. The depth where the state of strain switches from downdip extension to downdip compression is constrained at 110–125 km for the southernmost Ryukyu slab.

Based on our results, it is suggested that the subducted Philippine Sea plate beneath NE Taiwan plays a significant role in the overall orogenic process of the Taiwan region. We propose that the lithospheric collision in Taiwan consists of at least two major components: one is the well-recognized "arc–continent collision" that dominates central and southern Taiwan and the other the "slab–continent collision" that reigns in northern Taiwan.

The earthquake cluster near the Hualien area holds the key to understanding exactly how the subduction polarity flips from the Ryukyu to Luzon subduction zones. If the shallowly dipping nodal planes are the actual fault planes, then we can interpret these events as a manifestation of the formation of a diffuse interface thrust zone in the area. In other words, an incipient west- or northwestward subduction of the Philippine Sea plate is currently taking place beneath the Hualien area such that the geometric relation between the two plates is reversed with respect to the rest of the Longitudinal Valley. Alternatively, if we take the steeply dipping nodal planes as the fault planes, then these events probably imply that the steeply east-dipping Longitudinal Valley fault may have transformed into a diffuse thrust zone which eventually connects itself to the plate interplate beneath the southernmost Ryukyu arc, thus completing the polarity flip.

Both our results and the most recent GPS surveys indicate that the movement of western Taiwan seems to have a systematic southwestward component increasing from north to south. This phenomenon of lateral extrusion is particularly prominent in SW Taiwan, yet is not evident from either the strata of Quaternary deformation inland or marine morphology offshore, suggesting that the lateral extrusion process, if any, must have developed only recently. We conclude that the Coastal Plain of SW Taiwan is currently moving westward and/or the southern Henchung Peninsula is moving southward with respect to the Central Range and that the lateral extrusion is probably only a secondary feature in the tectonic processes of Taiwan.

Acknowledgements

We benefited from discussions with Jacques Angelier, Chung-Pai Chang, Wang-Ping Chen, Lin-Yun Chiao, Shu-Kun Hsu, Jyr-Ching Hu, Chi-Yue Huang, Serge Lallemand, Jian-Cheng

Lee, Cheng-Horng Lin, Chai-Yu Lu, Kuo-Fong Ma, Ruey-Juin Rau, Louis S. Teng, and Francis T. Wu. Comments from Louis Dorbath, Bertrand Delouis, and an anonymous reviewer significantly improve the manuscript. The technical staff of IES led by Chun-Chi Liu assumes the primary responsibility of maintaining BATS. Some figures are generated by the GMT software written by Paul Wessel and Walter H.F. Smith. The revision of this manuscript was completed in the Earthquake Research Institute (ERI), University of Tokyo, where one of the authors (H.K.) was invited under the Visiting Professor Program. The facilities and assistance provided by Prof. Yoshio Fukao and his colleagues are greatly appreciated. This research was supported by the National Science Council, ROC, grants NSC87-2116-M-001-001 and NSC88-2116-M-001-027.

Appendix A

The following figures, numbered according to their order of appearance in Table 1, show the complete results of our waveform inversion. Seismograms of three components (V: vertical; R: radial; T: transverse) from at least three BATS stations are used. The station code, azimuth, epicentral distance, name of velocity model, and the frequency band used in the inversion are shown at the top of each set of seismograms. Thick and thin traces denote observed and synthetic waveforms, respectively. The normalized maximum amplitude and corresponding misfit are near the beginning of each trace. The absolute amplitude scale is shown near the bottom. The focal mechanism is shown in lower-hemisphere projection with shaded area showing compressional P first motions. Dashed lines represent the corresponding best double-couple solution. Solid dots mark the *P*-, *T*-, and *B*-axes, while the open triangles show projected locations of used BATS stations. The plot of misfit versus focal depth is near the lower-right corner of each figure. The source time function (STF) is assumed to be a simple triangle of 2 s. An electronic version of this appendix is also available from BATS world-wide web site (http://www.earth.sinica.edu.tw/~spyder/index.html) or the anonymous ftp server of the Institute of Earth Sciences, Academia Sinica (140.109.80.235).

References

Angelier, J., Barrier, E., Chu, H.-T., 1986. Plate collision and paleostress trajectories in a fold–thrust belt: the foothills of Taiwan. Tectonophysics 125, 161–178.

Angelier, J. et al., 1995. Crustal extension in an active orogen: Taiwan. Proceedings of the 3rd Sino-French Symposium on Active Collision in Taiwan. Geological Society of China, Taipei, pp. 25–32.

Armijo, R., Tapponnier, P., Mercier, J.L., Han, T.-L., 1986. Quaternary extension in southern Tibet: field observations and tectonic implications. J. Geophys. Res. 91, 13,803–13,872.

Burchfiel, B.C., Royden, L.H., 1985. North–South extension within the convergent Himalayan region. Geology 13, 679–682.

Chemenda, A.I., 1995. Possible evolutionary model for the Taiwan collision explaining rock exhumation and extension in the Central Range. Proceedings of the 3rd Sino-French Symposium on Active Collision in Taiwan. Geological Society of China, Taipei, pp. 41–47.

Chemenda, A.I., Yang, R.K., Hsieh, C.H., Groholsky, A.L., 1997. Evolutionary model for the Taiwan collision based on physical modelling. Tectonophysics 274, 253–274.

Cheng, S.-N., 1995. The study of stress distribution in and around Taiwan. PhD thesis, National Central University, Chung Li, Taiwan.

Crespi, J.M., Chan, Y.-C., Swaim, M.S., 1996. Synorogenic extension and exhumation of the Taiwan hinterland. Geology 24, 247–250.

Dahlen, F.A., 1988. Mechanical energy budget of a fold-and-thrust belt. Nature 331, 335–337.

Dahlen, F.A., 1990. Critical taper model of fold-and-thrust belts and accretionary wedges. Annu. Rev. Earth Planet. Sci. 18, 55–99.

Dahlen, F.A., Suppe, J., Davis, D.M., 1984. Mechanics of fold-and-thrust belts and accretionary wedges: cohesive Coulomb theory. J. Geophys. Res. 89, 10,087–10,101.

Davis, D., Suppe, J., Dahlen, F.A., 1983. Mechanics of fold-and-thrust belts and accretionary wedges. J. Geophys. Res. 88, 1153–1172.

Dewey, J.F., Bird, J.M., 1970. Mountain belts and the new global tectonics. J. Geophys. Res. 75, 2625–2647.

England, P., Houseman, G., 1989. Extension during continental convergence, with application to the Tibetan Plateau. J. Geophys. Res. 94, 17,561–17,579.

Forsyth, D.W., 1983. Seismicity, focal mechanisms, and tectonics. Rev. Geophys. Res. 21, 1285–1291.

Fuh, S.-C., Liu, C.-S., 1998. Evolution of the Southern Longitudinal Trough in the incipient Taiwan arc–continent collision zone and its tectonic implication. J. Geol. Soc. China 41, 497–516.

Fuh, S.-C., Liu, C.-S., Lundberg, N., Reed, D.L., 1997. Strike-slip faults offshore southern Taiwan: implications for the oblique arc–continent collision processes. Tectonophysics 274, 25–39.

Ho, C.S., 1986. A synthesis of the geologic evolution of Taiwan. Tectonophysics 125, 1–16.

Hsu, S.-K., Sibuet, J.-C., 1995. Is Taiwan the result of arc–continent or arc–arc collision?. Earth Planet. Sci. Lett. 136, 315–324.

Hu, J.-C., Angelier, J., Lee, J.-C., Chu, H.-T., Byrne, D., 1996. Kinematics of convergence, deformation and stress distribution in the Taiwan collision area: 2-D finite-element numerical modelling. Tectonophysics 255, 243–268.

Huang, C.-Y., Wu, W.-Y., Chang, C.-P., Tsao, S., Yuan, P.B., Lin, C.-W., Xia, K.-Y., 1997. Tectonic evolution of accretionary prism in the arc–continent collision terrane of Taiwan. Tectonophysics 281, 31–51.

Isacks, B., Oliver, J., Sykes, L.R., 1968. Seismology and the new global tectonics. J. Geophys. Res. 73, 5855–5899.

Kao, H., Chen, W.-P., 1991. Earthquakes along the Ryukyu–Kyushu arc: strain segmentation, lateral compression, and the thermomechanical state of the plate interface. J. Geophys. Res. 96, 21,443–21,485.

Kao, H., Wu, F.T., 1996. The 16 September 1994 earthquake (m_b = 6.5) in the Taiwan strait and its tectonic implications. Terr. Atmos. Oceanic Sci. 7, 13–29.

Kao, H., Jian, J.-R., 1999. Source parameters of regional earthquakes in Taiwan: July 1995–December 1996. Terr. Atomos. Oceanic Sci. 10, 585–604.

Kao, H., Jian, P.-R., Ma, K.-F., Huang, B.-S., Liu, C.-C., 1998a. Moment-tensor inversion for offshore earthquakes east of Taiwan and their implications to regional collision. Geophys. Res. Lett. 25, 3619–3622.

Kao, H., Shen, S.J., Ma, K.-F., 1998b. Transition from oblique subduction to collision: earthquakes in the southernmost Ryukyu arc–Taiwan region. J. Geophys. Res. 103, 7211–7229.

Kao, H., Huang, G.-C., Liu, C.-S., 2000. Transition from oblique subduction to collision in the northern Luzon arc–Taiwan region: constraints from bathymetery and seismic observations. J. Geophys. Res. 105, 3059–3079.

Lacombe, O., Mouthereau, F., Deffontaines, B., Angelier, J., 1999. Structural, geodetic and seismological evidence for tectonic escape in SW Taiwan: a tentative geometric model. Proceedings of the 4th French-Taiwan Symposium on Active Subduction and Collision in Southeast Asia. University of Montpellier II, Montpellier, pp. 87–91.

Lin, C.-H., Yeh, Y.-H., Yen, H.-Y., Chen, K.-C., Huang, B.-S., 1998. Three-dimensional elastic wave velocity structure of the Hualien region of Taiwan: evidence of active crustal exhumation. Tectonics 17, 89–103.

Liu, C.-C., 1995. The Ilan plain and the southwestward extending Okinawa trough. J. Geol. Soc. China 38, 229–242.

Liu, C.-S., Huang, I.L., Teng, L.S., 1997. Structural features off southwestern Taiwan. Mar. Geol. 137, 305–319.

Lu, C.-Y., Hsü, K.J., 1992. Tectonic evolution of the Taiwan mountain belt. Pet. Geol. Taiwan 27, 21–46.

Lundberg, N., Reed, D.L., Liu, C.-S., Lieske, J.J., 1997. Forearc-basin closure and arc accretion in the submarine suture zone south of Taiwan. Tectonophysics 274, 5–23.

Ma, K.-F., Wang, J.-H., Zhao, D., 1996. Three-dimensional seismic velocity structure of the crust and uppermost mantle beneath Taiwan. J. Phys. Earth 44, 85–105.

Miki, M., Matsuda, T., Otofuji, Y., 1990. Opening mode of the Okinawa Trough: palemagnetic evidence from the South Ryukyu Arc. Tectonophysics 175, 335–347.

Molnar, P., Tapponnier, P., 1978. Active tectonics of Tibet. J. Geophys. Res. 83, 5361–5375.

Ni, J., York, J.E., 1978. Late Cenozoic tectonics of the Tibetan plateau. J. Geophys. Res. 83, 5377–5384.

Ratschbacher, L., Frisch, W., Liu, G., Chen, C., 1994. Distributed deformation in southern and western Tibet during and after the India–Asia collision. J. Geophys. Res. 99, 19,917–19,945.

Rau, R.-J., 1996. 3-D seismic tomography, focal mechanisms, and Taiwan orogeny. PhD thesis, State University of New York, Binghamton.

Rau, R.-J., Wu, F.T., 1995. Tomographic imaging of lithospheric structures under Taiwan. Earth Planet. Sci. Lett. 133, 517–532.

Rau, R.-J., Wu, F.T., Shin, T.-C., 1996. Regional network focal mechanism determination using 3D velocity model and SH/P amplitude ratio. Bull. Seismol. Soc. Am. 86, 1270–1283.

Seno, T., Stein, S., Gripp, A.E., 1993. A model for the motion of the Philippine Sea Plate consistent with NUVEL-1 and geological data. J. Geophys. Res. 98, 17,941–17,948.

Sibuet, J.-C., Letouzey, J., Barbier, F., Charvet, J., Foucher, J.-P., Hilde, T.W.C., Kimura, M., Chiao, L.-Y., Marsset, B., Muller, C., Stephan, J.-F., 1987. Back arc extension in the Okinawa trough. J. Geophys. Res. 92, 14,041–14,063.

Sibuet, J.-C., Deffontaines, B., Hsu, S.-K., Thareau, N., Le Formal, J.-P., Liu, C.-S., ACT party, 1998. Okinawa trough backarc basin: early tectonic and magmatic evolution. J. Geophys. Res. 103, 30,245–30,267.

Suppe, J., 1980. A retrodeformable cross section of northern Taiwan. Proc. Geol. Soc. China 23, 46–55.

Suppe, J., 1981. Mechanics of mountain building and metamorphism in Taiwan. Mem. Geol. Soc. China 4, 67–89.

Suppe, J., 1984. Kinematics of arc–continent collision, flipping of subduction, and back-arc spreading near Taiwan. Mem. Geol. Soc. China 6, 21–33.

Tapponnier, P., Molnar, P., 1977. Active faulting and tectonics in China. J. Geophys. Res. 82, 2905–2930.

Tapponnier, P., Mercier, J.L., Armijo, R., Han, T., Zhou, J., 1981. Field evidence for active normal faulting in Tibet. Nature 294, 410–414.

Teng, L.S., 1990. Geotectonic evolution of late Cenozoic arc–continent collision. Tectonophysics 183, 57–76.

Teng, L.S., 1996. Extensional collapse of the northern Taiwan mountain belt. Geology 24, 949–952.

Tsai, Y.-B., 1986. Seismotectonics of Taiwan. Tectonophysics 125, 17–37.

Tsai, Y.-B., Teng, T., Chiu, J.-M., Liu, H.-L., 1977. Tectonic implications of the seismicity in the Taiwan region. Mem. Geol. Soc. China 2, 13–41.

Uyeda, S., Kanamori, H., 1979. Back-arc opening and the mode of subduction. J. Geophys. Res. 84, 1049–1061.

Wang, C.-Y., Chen, K.-P., 1997. A seismic refraction profile across the Longitudinal Valley near Hualien, Taiwan. Terr. Atmos. Oceanic Sci. 8, 295–312.

Waschbusch, P., Beaumont, C., 1996. Effect of a retreating subduction zone on deformation in simple regions of plate convergence. J. Geophys. Res. 101, 28,133–28,148.

Wu, F.T., 1978. Recent tectonics of Taiwan. J. Phys. Earth 26 (Suppl.), S265–S299.

Wu, F.T., Rau, R.-J., Salzberg, D., 1997. Taiwan orogeny: thin-skinned or lithospheric collision. Tectonophysics 274, 191–220.

Yeh, Y.-H., Lin, C.-H., Roecker, S.W., 1989. A study of upper crustal structures beneath northeastern Taiwan: possible evidence of the western extension of Okinawa trough. Proc. Geol. Soc. China 32 (2), 139–156.

Yeh, Y.-H., Barrier, E., Lin, C.-H., Angelier, J., 1991. Stress tensor analysis in the Taiwan area from focal mechanisms of earthquakes. Tectonophysics 200, 267–280.

Yu, S.-B., Liu, C.-C., 1989. Fault creep in the central segment of the Longitudinal Valley Fault, eastern Taiwan. Proc. Geol. Soc. China 32 (3), 209–231.

Yu, S.-B., Chen, H.-Y., Kuo, L.-C., 1997. Velocity field of GPS stations in the Taiwan area. Tectonophysics 274, 41–59.